Inherent control error in a multi-PD controlled double inverted pendulum

Gergely Gyebrószki[†], Gábor Csernák[*]
[†]*Department of Applied Mechanics, Budapest University of Technology and Economics Budapest, Hungary*
[*]*MTA-BME Research Group on Dynamics of Machines and Vehicles, Budapest, Hungary.*

Summary. Micro-chaos is a phenomenon, when digital effects (sampling, round-off and delay) cause small amplitude chaotic oscillations. Digital effects are often neglected or considered as a noise, however, micro-chaos is a deterministic source of control error. In this paper, we investigate a multi-PD controlled double inverted pendulum and show the micro-chaotic behaviour in case of rounding and sampling. For the estimation of quantization-induced control error, a universal error estimation method is presented and it is shown, that the estimates provide a good initial state space region for cell mapping methods.

Multi-PD controlled double inverted pendulum

Consider a double inverted pendulum with a control torque at the lower joint (Fig. 1, left). Given a multi PD-control with zero order hold, τ sampling time, and rounding of the control signal, the torque between the i^{th} and $i+1^{\text{st}}$ sampling instances can be written as:

$$M = \rho_{\text{M}}\,\text{Int}\left(\frac{1}{\rho_{\text{M}}}\underbrace{\left(p_1\,\varphi_1(t_i)+d_1\,\dot{\varphi}_1(t_i)+p_2\,\varphi_2(t_i)+d_2\,\dot{\varphi}_2(t_i)\right)}_{:=m(t_i)}\right), \quad t_i = t_0 + i\,\tau. \tag{1}$$

Here p_1, p_2, d_1, d_2 are control gains, and ρ_{M} is the resolution of the control torque. After linearization, the equation of motion can be solved between successive sampling instants. Introducing dimensionless time $\hat{t} = t/\tau$ and rearranging the solution of the equation of motion, we obtain the following *micro-chaos* map, that describes the state of the pendulum at successive sampling instants:

$$\mathbf{y}_{i+1} = \mathbf{U}\,\mathbf{y}_i + \mathbf{b}\,M, \tag{2}$$

where: $\mathbf{y}_i^{\text{T}} = \begin{pmatrix} \dot{\varphi}_1(t_i) & \dot{\varphi}_2(t_i) & \varphi_1(t_i) & \varphi_2(t_i) \end{pmatrix}$. $\mathbf{U}$ and $\mathbf{b}$ are composed from the solution:

$$\mathbf{U} = \begin{bmatrix} \frac{A_{12}c_2-A_{22}c_1}{A_{12}-A_{22}} & \frac{c_1-c_2}{A_{12}-A_{22}} & \frac{A_{22}\alpha_1 s_1-A_{12}\alpha_2 s_2}{A_{12}-A_{22}} & \frac{\alpha_2 s_2-\alpha_1 s_1}{A_{12}-A_{22}} \\ \frac{A_{12}A_{22}(c_2-c_1)}{A_{12}-A_{22}} & \frac{A_{12}c_1-A_{22}c_2}{A_{12}-A_{22}} & \frac{A_{12}A_{22}(\alpha_1 s_1-\alpha_2 s_2)}{A_{12}-A_{22}} & \frac{A_{22}\alpha_2 s_2-A_{12}\alpha_1 s_1}{A_{12}-A_{22}} \\ \frac{A_{12}\alpha_1 s_2-A_{22}\alpha_2 s_1}{A_{12}\alpha_1\alpha_2-A_{22}\alpha_1\alpha_2} & \frac{\alpha_2 s_1-\alpha_1 s_2}{A_{12}\alpha_1\alpha_2-A_{22}\alpha_1\alpha_2} & \frac{A_{12}c_2-A_{22}c_1}{A_{12}-A_{22}} & \frac{c_1-c_2}{A_{12}-A_{22}} \\ \frac{A_{12}A_{22}\alpha_1 s_2-A_{12}A_{22}\alpha_2 s_1}{A_{12}\alpha_1\alpha_2-A_{22}\alpha_1\alpha_2} & \frac{A_{12}\alpha_2 s_1-A_{22}\alpha_1 s_2}{A_{12}\alpha_1\alpha_2-A_{22}\alpha_1\alpha_2} & \frac{A_{12}A_{22}(c_2-c_1)}{A_{12}-A_{22}} & \frac{A_{12}c_1-A_{22}c_2}{A_{12}-A_{22}} \end{bmatrix},$$

$$\mathbf{b}^{\text{T}} = \begin{bmatrix} \frac{A_{22}\,s_1}{\alpha_1(A_{12}-A_{22})} & \frac{A_{12}\,s_2}{\alpha_2(A_{22}-A_{12})} & \frac{A_{22}\,c_1 i}{\alpha_1(A_{12}-A_{22})} & \frac{A_{12}\,c_2 i}{\alpha_2(A_{22}-A_{12})} \end{bmatrix}.$$

Here α_1, α_2 are the angular natural frequencies, c_i and s_i are $\cosh(\alpha_i)$ and $\sinh(\alpha_i)$ respectively, and A_{12} and A_{22} are the 2^{nd} components of the mode shape vectors (with the first component taken as $A_{i,1} = 1$).

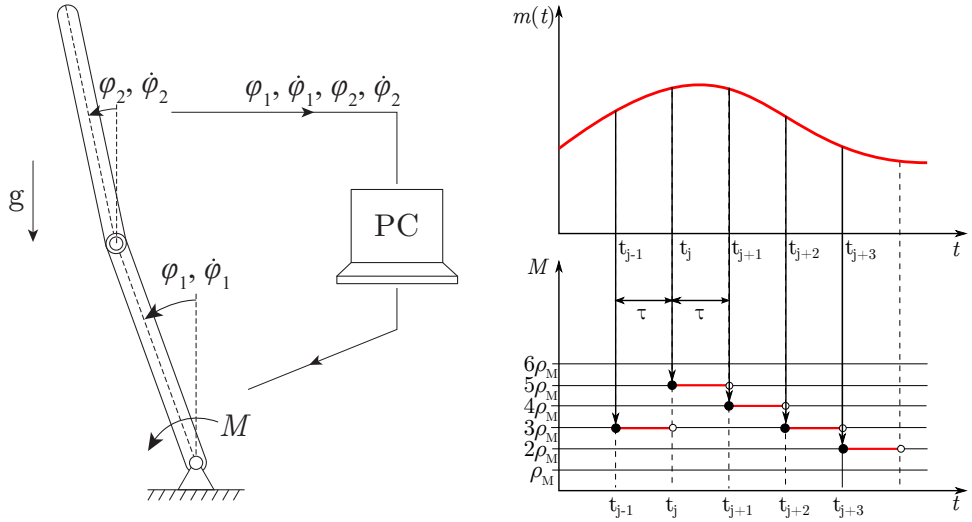

Figure 1: Double inverted pendulum with control torque and zero order hold multi-PD control. The calculated control effort $m(t)$ is rounded due to the quantization of the control torque. See Eq. (1).

Stable parameter region of multi-PD control

Considering the stability of the multi-PD control, one can calculate the 4D parameter region (See Fig. 2.) corresponding to stable equilibrium solution for the sampled, but not rounded case at $\varphi_1 = 0$, $\varphi_2 = 0$, using the Jury's stability criterion. If the rounding is taken into account, the stabilized equilibrium becomes unstable, as the control turns off in the band corresponding to $M = 0$, although the equilibrium remains practically stable outside the $M = 0$ band. Therefore, we are interested in the practical stability of the micro-chaos map and the maximum distance from the origin is examined.
It is important to note, that a stabilizing control can be achieved with p_1 turned off. This enables us to examine solutions and switching planes defined by Eq. (1) in a 3D subspace of the parameter-space. (See Fig. 3.)

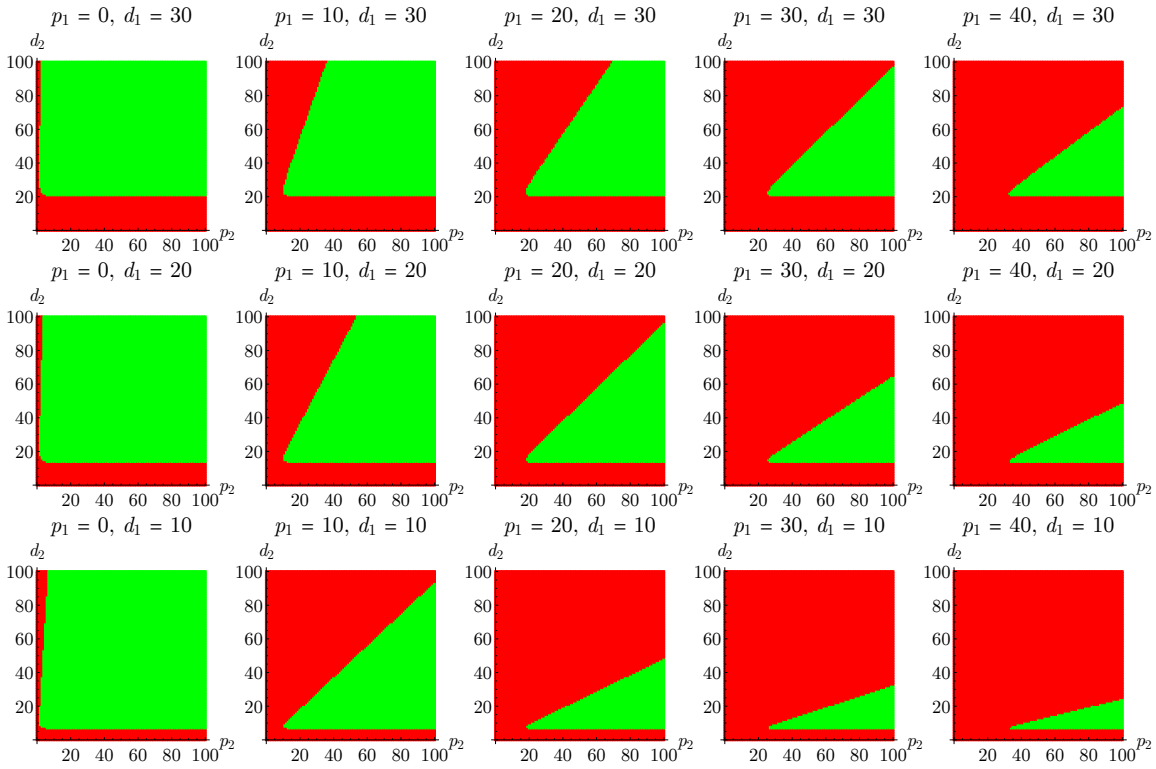

Figure 2: Stable parameter domain of the multi-PD control. Green ■ indicates stable, red ■ indicates unstable parameter regions.

Micro-chaotic behaviour

The rounding in the micro-chaos map defines switching surfaces, which separate bands with the same integer result of the rounding function (See Eq. (1)). For a given torque-resolution, increasing the sampling time τ allows the system to venture into a neighbouring band to some extent, before the next sampling occurs and the control torque is updated.
This results in chaotic behaviour, as the time spent and the position of entries and exits vary during the motion between adjacent bands [4]. An example attractor, where the solution visits the $M = -\rho_{\mathrm{M}}$, $M = 0$ and $M = \rho_{\mathrm{M}}$ bands can be seen in Fig. 3.
In case of system parameters corresponding to larger sampling times or smaller torque-resolution, the system can cross multiple control bands before the next sampling occurs (and the value of M gets updated).

Estimation of error in the micro-chaos map

Rewrite the micro-chaos map into the following form:

$$\mathbf{y}_{i+1} = \mathbf{S}\,\mathbf{y}_i - \mathbf{b}\,\chi_i \tag{3}$$

where $\mathbf{S} = \mathbf{U} + \mathbf{b} \otimes [d_1\, d_2\, p_1\, p_2]$ is the map corresponding to the stabilized system and χ_i denotes the fractional part removed during the i^{th} rounding. Let us examine the state $\mathbf{y}_i$, $i \to \infty$, with expanding the application of the map:

$$\lim_{i\to\infty}\left(\mathbf{S}^i\,\mathbf{y}_0 - \sum_{k=0}^{i-1}\mathbf{S}^k\,\mathbf{b}\,\chi_k\right) = \lim_{i\to\infty}\left(-\sum_{k=0}^{i-1}\mathbf{S}^k\,\mathbf{b}\,\chi_k\right),$$

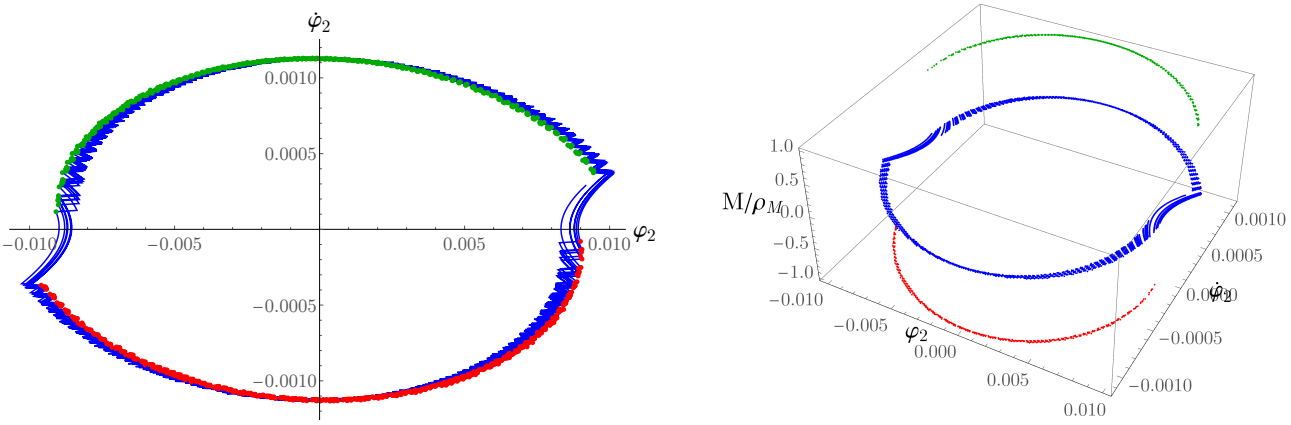

Figure 3: Example attractor of the micro-chaos map, colours indicate different M values. Red ■, blue ■ and green ■ colours indicate $\mathrm{M}/\rho_{\mathrm{M}} = -1,\ 0,\ +1$ values. On the left image, the points of the attractor are joined with blue lines.

because $\lim_{i\to\infty} \mathbf{S}^i = \mathbf{0}$ is required for stability, (see [2]). Introducing $\mathbf{D}$ and $\mathbf{T}$ as the diagonal matrix of eigenvalues (λ_i) and matrix of eigenvectors of $\mathbf{S}$, respectively, one can write:

$$\mathbf{y}_\infty = -\mathbf{T} \sum_{k=0}^{\infty} \mathbf{D}^k\, \mathbf{T}^{-1}\, \mathbf{b}\, \chi_k. \tag{4}$$

Here $\mathbf{y}_\infty$ denotes the limit of all possible solutions (i.e. after transient behaviour disappears). Let ϕ_i and ρ_i denote the modulus and argument of the i^{th} eigenvalue λ_i, and $\tilde{\mathbf{b}} = \mathbf{T}^{-1}\,\mathbf{b}$. With this notation Eq. (4) can be written as:

$$\mathbf{y}_\infty = -\mathbf{T} \begin{bmatrix} \sum_{k=0}^{\infty} \lambda_1^k\, \chi_k\, \tilde{b}_1 \\ \sum_{k=0}^{\infty} \lambda_2^k\, \chi_k\, \tilde{b}_2 \\ \vdots \\ \sum_{k=0}^{\infty} \lambda_n^k\, \chi_k\, \tilde{b}_n \end{bmatrix} = - \begin{bmatrix} \sum_{k=0}^{\infty} \sum_{j=1}^{n} T_{1,j} \lambda_j^k\, \chi_k\, \tilde{b}_j \\ \sum_{k=0}^{\infty} \sum_{j=1}^{n} T_{2,j} \lambda_j^k\, \chi_k\, \tilde{b}_j \\ \vdots \\ \sum_{k=0}^{\infty} \sum_{j=1}^{n} T_{n,j} \lambda_j^k\, \chi_k\, \tilde{b}_j \end{bmatrix} =$$

$$- \begin{bmatrix} \sum_{k=0}^{\infty} \sum_{j=1}^{n} T_{1,j}\, \rho_j^k\, (\cos(k\,\phi_j) + i\, \sin(k\,\phi_j))\, \chi_k\, \tilde{b}_j \\ \sum_{k=0}^{\infty} \sum_{j=1}^{n} T_{2,j}\, \rho_j^k\, (\cos(k\,\phi_j) + i\, \sin(k\,\phi_j))\, \chi_k\, \tilde{b}_j \\ \vdots \\ \sum_{k=0}^{\infty} \sum_{j=1}^{n} T_{n,j}\, \rho_j^k\, (\cos(k\,\phi_j) + i\, \sin(k\,\phi_j))\, \chi_k\, \tilde{b}_j \end{bmatrix} := \begin{bmatrix} \sum_{k=0}^{\infty} \sigma_{1,k} \\ \sum_{k=0}^{\infty} \sigma_{2,k} \\ \vdots \\ \sum_{k=0}^{\infty} \sigma_{n,k} \end{bmatrix}. \tag{5}$$

Note, that in each component of $\mathbf{y}_\infty$, the expression denoted by $\sigma_{j,k}$ depend on the same χ_k fractional part. To maximize the i^{th} component of $\mathbf{y}_\infty$, a trivial choice of the k^{th} fractional part $\chi_k = \text{sign}(\sigma_{i,k})$ can be made [1], yielding a good upper estimation when compared to simulated results, see Fig 4.

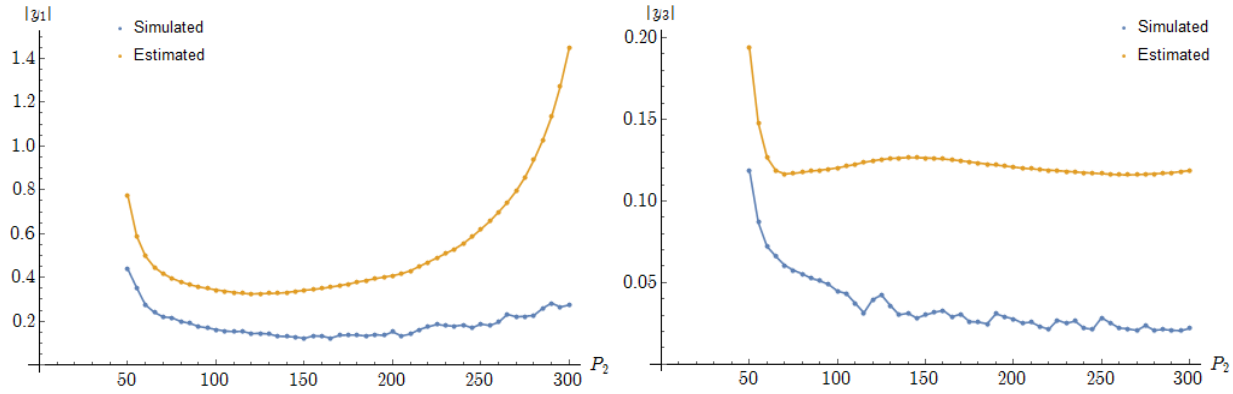

Figure 4: Comparison of simulated and estimated maxima for $y_1 = \dot{\varphi}_1$ and $y_3 = \varphi_1$.

One can also construct a suboptimal choice of χ_k to estimate the maximum $\mathfrak{L}_1$ norm. Let us rewrite Eq. (5) in the following form:

$$\mathbf{y}_\infty = \begin{bmatrix} \sum_{k=0}^{\infty} \sigma_{1,k} \\ \sum_{k=0}^{\infty} \sigma_{2,k} \\ \vdots \\ \sum_{k=0}^{\infty} \sigma_{n,k} \end{bmatrix} = \begin{bmatrix} \sum_{k=0}^{\infty} e_{1,k}\,\chi_k \\ \sum_{k=0}^{\infty} e_{2,k}\,\chi_k \\ \vdots \\ \sum_{k=0}^{\infty} e_{n,k}\,\chi_k \end{bmatrix} = \begin{bmatrix} s_{1,m} + \sum_{k=m+1}^{\infty} e_{1,k}\,\chi_k \\ s_{2,m} + \sum_{k=m+1}^{\infty} e_{2,k}\,\chi_k \\ \vdots \\ s_{n,m} + \sum_{k=m+1}^{\infty} e_{n,k}\,\chi_k \end{bmatrix}. \tag{6}$$

Where $s_{j,m}$ denotes $\sum_{k=0}^{m} e_{j,k}\,\chi_k$. Utilizing the strategy which ensures, that the k^{th} fractional part χ_k is chosen, such that the new terms maximize the increase of the L_1 norm in the k^{th} step, taking into account the sign of the already accumulated part of the series, one can write:

$$\chi_k = \operatorname{sign}(\operatorname{sign}(s_{1,k-1})\,e_{1,k} + \operatorname{sign}(s_{2,k-1})\,e_{2,k} + \cdots + \operatorname{sign}(s_{n,k-1})\,e_{n,k}) = \operatorname{sign}(\operatorname{sign}(\mathbf{s}_k)^{\mathrm{T}}\,\mathbf{e}_k). \tag{7}$$

Although the rule for the choice of χ_k described by Eq. (7) does not yield the optimal choice to maximize the L_1 norm of $\mathbf{y}_\infty$, it provides a good estimation. We have generated the optimal χ_k series (yielding the maximum L_1 norm) for $k \in \{0 \ldots 100\}$ and compared it with the rule based estimation (See Fig. 5.) and found that the rule based estimation yields close results to the optimal one. It is important to note, that generating the optimal χ_k series involves exponential time complexity, as the number of combinations is 2^l for a given series length l.

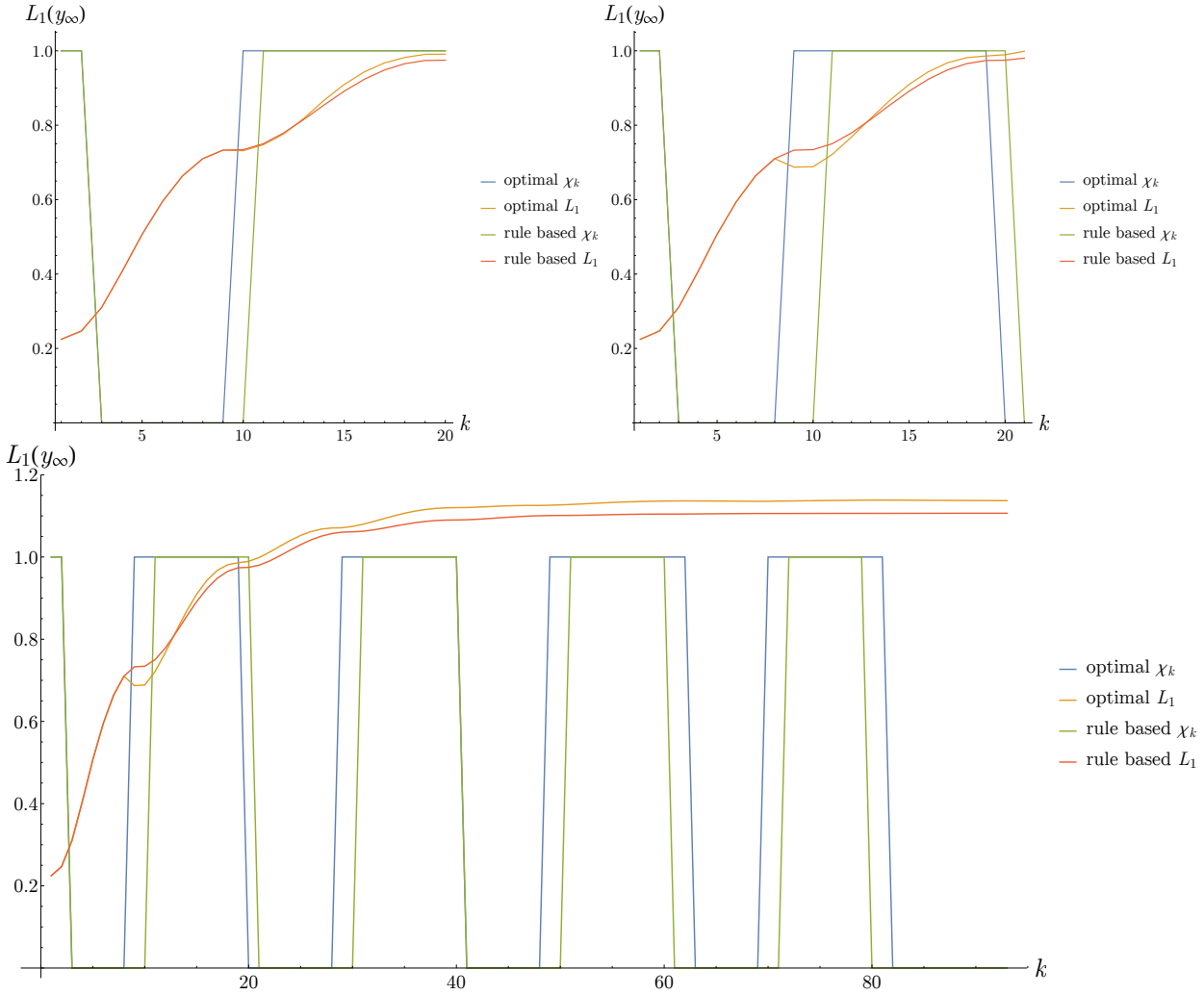

Figure 5: Analysis of rule-based $\mathfrak{L}_1$ norm estimation with: $\alpha_1 = 4.23763i$, $\alpha_2 = 11.3663i$, $A_{12} = 1.4305$, $A_{22} = -2.09717$. One can see, that the optimal χ_k combination incorporates a choice of χ_9 which decreases the $\mathfrak{L}_1$ norm locally, but increases its value overall. *Top left:* series length $k = 20$, *right:* $k = 21$, *bottom:* $k = 93$.

Application of Clustered Simple Cell Mapping

The estimated control errors can be used to choose the initial state space region for Clustered Simple Cell Mapping (SCM), which is used for further analysis of the micro-chaos map. An advantage of Clustered SCM is that it can expand the state space region in cases, when it does not contain all objects governing the dynamics of the map. This means, that the estimation of various norms can be used effectively, even if they are determined with minor inaccuracies (due to the truncating of the infinite series, or using the rule based estimation of $\mathfrak{L}_1$ norm, for example.) An example of application to the micro-chaos map Eq. (2). is shown on Fig. 6., which illustrates the result of Clustered SCM using a low resolution cell state space.

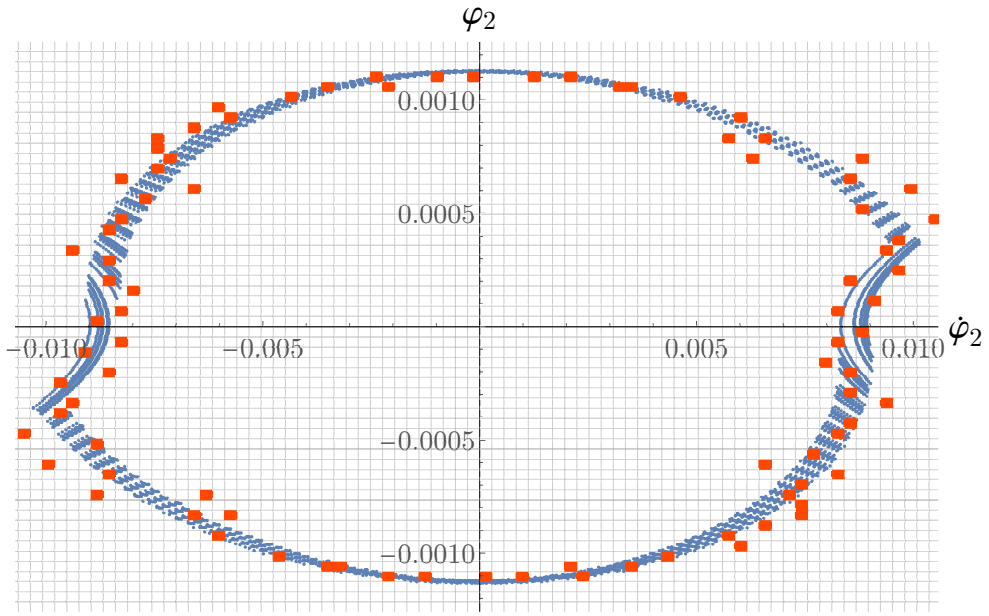

Figure 6: Clustered SCM results with a cell state space of $40 \times 100 \times 40 \times 60$ cells (total of 9.6 million cells). Orange ■ tiles indicate a periodic group of 92 cells situated on the attractor, blue ■ dots show the real attractor obtained with numerical simulation.

Conclusions

Digital effects can cause considerable error in control systems. We presented a simple double inverted pendulum and its corresponding micro-chaos map. A simple formulation of the control error was presented and compared to simulation results. A fast, but suboptimal estimation for the $\mathfrak{L}_1$ norm is described and it was shown that it yields acceptable estimation. The estimated control errors can be used to select an initial state space region when using Clustered Simple Cell Mapping, therefore aiding further analysis of the micro-chaos map.

References

[1] Gábor Csernák (2016) Quantization-induced control error in a digitally controlled system *Nonlinear Dynamics* **85**(4): 2749–2763

[2] Gábor Csernák, Gergely Gyebrószki, Gábor Stépán (2016) Multi-Baker Map as a Model of Digital PD Control *International Journal of Bifurcation and Chaos* **26**(2): 1650023-1–11.

[3] Gergely Gyebrószki, Gábor Csernák (2017) Clustered Simple Cell Mapping: An extension to the Simple Cell Mapping method *Communications in Nonlinear Science and Numerical Simulation* **42**: 607–622.

[4] Gábor Csernák, Gábor Stépán (2011) Sampling and Round-off, as Sources of Chaos in PD-controlled Systems *19th Mediterranean Conference on Control and Automation* Corfu, Greece, 1319–1324